Efficiency Enhancement in Free-Electron Lasers by Means of Concurrent rf Acceleration

H. P. Freund
Science Applications International Corp., McLean, Virginia 22102, USA

J. Pasour
Mission Research Corp., Newington, Virginia 22122, USA

(Received 14 April 2003; published 29 August 2003)

Efficiency enhancement in free-electron lasers (FELs) using rf beam acceleration in the wiggler is described. Since the beam tube is a waveguide, there are low and high frequency resonances. Injection of low frequency power can act as an inverse-FEL accelerator concurrently with high frequency power extraction. Simulation of a FEL using this technique shows that substantial efficiency enhancements are possible without significant increases in the beam energy spread, which facilitates the use of energy recovery schemes. The technique is applicable to amplifier and oscillator configurations.

DOI: 10.1103/PhysRevLett.91.094801 PACS numbers: 41.60.Cr, 52.59.Rz

Free-electron lasers (FELs) have operated over virtually the entire electromagnetic spectrum [1–4]. At present, there are two directions for FEL development. One is to extend the spectral range to short wavelengths and the coherent production of x rays [3,4]. Another is high average power operation in the infrared through ultraviolet spectra. To this end, a major accomplishment was the production of 2.1 kW at a wavelength of 3 μm at the Thomas Jefferson National Accelerator Facility [5]. A barrier in the achievement of higher powers is the average charge and brightness limitations with electron injectors. However, the use of efficiency enhancement could reduce the charge needed for any desired level of output power.

The most common means of efficiency enhancement is a tapered wiggler. When the wiggler amplitude and/or period is tapered downward over the course of the wiggler, then the amplitude of the wiggler-induced transverse motion decreases and the axial velocity increases. This axial acceleration of the beam maintains the FEL resonance over an extended interaction length and permits the extraction of more energy from the beam. However, the drawback to this technique is that the only part of the beam that participates in the tapered wiggler interaction is the fraction trapped by the ponderomotive wave formed by the beating of the wiggler and radiation fields. It is this part of the beam that loses energy to the radiation resulting in a double humped spent beam distribution.

In order to circumvent the large overall energy spread inherent in tapered wiggler techniques, we propose to enhance the efficiency by the concurrent rf acceleration of the beam in the wiggler. Both dc [6] and rf [7,8] acceleration schemes have been proposed. In the dc scheme, an external potential drop is imposed along the axis of the wiggler and this was shown, in theory and simulation, to result in substantial efficiency enhancements. While the spent beam energy was not addressed in these analyses, this energy spread is likely to be relatively small since the potential acts uniformly on the entire beam. Unfortunately, there are practical difficulties in the application of a dc potential along the wiggler axis. An rf acceleration scheme using a slow-wave accelerating structure [7,8] was shown in theory to be feasible, although the question of the resulting energy spread was, again, not addressed. However, an rf cavity is a complex structure that is inconsistent with the creation of large amplitude wiggler fields, which requires a small wiggler gap (i.e., the distance between the jaws of a planar wiggler). However, instead of using a slow-wave rf cavity it is possible to make use of the low frequency (long wavelength) FEL resonance in a smooth-bore beam tube to accelerate the beam.

A beam tube is also a waveguide that cannot propagate wavelengths that are much longer than the transverse dimensions of the tube. Such a structure supports a complex collection of transverse modes. The dispersion equation is hyperbolic and approaches the light line asymptotically at high frequencies, i.e., $\omega^2 = c^2k^2 + \omega_{\rm co}^2$, for angular frequency ω, wavelength k, and cutoff frequency $\omega_{\rm co}$. As a result, there are two intersections with the FEL resonance line $\omega = (k + k_w)v_b$, where k_w is the wiggler wave number, and v_b is the bulk axial beam velocity. This is illustrated schematically in Fig. 1. The upper (ω_+) and lower (ω_-) intersection frequencies are

$$\omega_\pm = \gamma_b^2 k_w v_b \left[1 \pm \beta_b \sqrt{1 - \frac{\omega_{\rm co}^2}{\gamma_b^2 k_w^2 v_b^2}} \right], \qquad (1)$$

where $\gamma_b = (1 - v_b^2/c^2)^{-1/2}$ is the relativistic factor. Note that $\omega_+ \to 2\gamma_b^2 k_w v_b$ as expected when $\omega_{\rm co} \ll \omega_+$.

For convenience, we deal with the TE modes in cylindrical drift tubes. Weaker interactions are also possible with TM modes but will not be treated here. Further, since some FELs employ rectangular beam tubes within the wiggler, the analysis can easily be reformulated to treat these structures as well. The vector potential of the TE_{ln} mode is given in cylindrical coordinates by

$$\mathbf{A}_{ln} = \hat{A}_{ln} \left[\frac{l}{\kappa_{ln} r} J_l(\kappa_{ln} r) \hat{\mathbf{e}}_r \sin\alpha_l + J_l'(\kappa_{ln} r) \hat{\mathbf{e}}_\theta \cos\alpha_l \right], \quad (2)$$

where $\alpha_l = kz + l\theta - \omega t$ is the phase, J_l is the regular Bessel function of the first kind of order l, κ_{ln} is the cutoff wave number ($= x_{ln}/R_g$, where R_g is the waveguide radius and x_{ln} is the nth zero of J_l) so that $\omega_{co} = \kappa_{ln}c$. The initial field amplitude can be related to the injected power in the mode, P_{ln}, via

$$\frac{e\hat{A}_{ln}}{m_e c^2} = \frac{\sqrt{c\kappa_{ln}^2/\omega k}}{\sqrt{x_{ln}^2 - l^2}} \frac{1}{J_l'(x_{ln})} \left(\frac{P_{ln}}{1.088\,74\ \text{GW}}\right)^{1/2}. \quad (3)$$

For simulation purposes, this acceleration model has been incorporated into the 3D FEL simulation code MEDUSA [9], which models both planar and helical wiggler geometry and treats the electromagnetic field as a superposition of Gaussian modes. The field equations are integrated simultaneously with the 3D Lorentz force equations for an ensemble of electrons. No wiggler-average orbit approximation is used, and MEDUSA can propagate the electron beam through a complex wiggler/transport line including multiple wiggler sections, quadrupole and dipole corrector magnets, focusing/defocusing lattices, and magnetic chicanes. The rf acceleration is included in the MEDUSA simulation by the relatively simple expedient of adding the force due to the TE_{ln} mode to the integration of the particle trajectories. The electric and magnetic fields for the TE_{ln} mode can be derived from this vector potential, and the force on the electrons due to these fields is

$$\mathbf{F}_{ln} = -\frac{e}{2c}\hat{A}_{ln}\{\hat{\mathbf{e}}_x[(\omega - k\mathbf{v}_z)C_{ln}^{(+)} - k\mathbf{v}_y J_l(\kappa_{ln}r)\cos\alpha_l] - \hat{\mathbf{e}}_y[(\omega - k\mathbf{v}_z)S_{ln}^{(-)} - k\mathbf{v}_x J_l(\kappa_{ln}r)\cos\alpha_l] + k\hat{\mathbf{e}}_z(\mathbf{v}_x C_{ln}^{(+)} - \mathbf{v}_y S_{ln}^{(-)})\} + \frac{e}{2c}\hat{A}_{ln}\Gamma_{ln}\{\mathbf{v}_z(\hat{\mathbf{e}}_x S_{ln}^{(+)} + \hat{\mathbf{e}}_y C_{ln}^{(-)}) - \hat{\mathbf{e}}_z(\mathbf{v}_x S_{ln}^{(+)} + \mathbf{v}_y C_{ln}^{(-)})\}, \quad (4)$$

in rectangular coordinates, where Γ_{ln} is the damping (or growth) rate of the field, $C_{ln}^{(\pm)} = [J_{l-1}(\rho_{ln})\cos\alpha_{l-1} \pm J_{l+1}(\rho_{ln})\cos\alpha_{l+1}]$, $S_{ln}^{(\pm)} = [J_{l-1}(\rho_{ln})\sin\alpha_{l-1} \pm J_{l+1}(\rho_{ln})\sin\alpha_{l+1}]$, and $\rho_{ln} = \kappa_{ln}r$. The terms in Γ_{ln} are likely to be small since the growth, or damping, rate of the accelerating field will occur on much longer scale lengths than the wavelength.

Since the rf amplitude will decrease (increase) as the electrons are accelerated (decelerated), we must also include pump depletion in the formulation in MEDUSA. The change in the power in going from z to $z + \Delta z$ due to the TE_{ln} mode is given by

$$P_{ln}(z + \Delta z) = P_{ln}(z) - m_e c^2 \sum_{i=1}^{N_e}\left(\frac{d\gamma_i}{dt}\right), \quad (5)$$

where the sum is over all N_e (macro) electrons in the simulation, and

$$\frac{d\gamma}{dt} = -\frac{\omega}{2c}\frac{e\hat{A}_{ln}}{m_e c^2}(\mathbf{v}_x C_{ln}^{(+)} - \mathbf{v}_y S_{ln}^{(-)}) \quad (6)$$

describes the change in energy of each electron due to the rf field. Therefore, by summing over all the electrons at each step in z, we can calculate the change in the power of the field. This also permits us to determine the damping (or growth) rate since

$$\frac{dP_{ln}}{dz} = -\frac{m_e c^2}{\Delta z}\sum_{i=1}^{N_e}\left(\frac{d\gamma_i}{dt}\right) \quad (7)$$

and

$$\Gamma_{ln} = \frac{1}{\hat{A}_{ln}}\frac{d\hat{A}_{ln}}{dz} = \frac{1}{2P_{ln}}\frac{dP_{ln}}{dz}. \quad (8)$$

As a result, each step in the integration includes the acceleration or deceleration of the electrons due to the TE_{ln} mode and the concomitant evolution of the pump amplitude.

We consider an amplifier with an electron beam energy of 140 MeV, a peak current of 800 A, a normalized emittance of 1.9 mmrad, and an energy spread of 0.5%. The wiggler has a period of 2.18 cm with an on-axis amplitude of 10.098 kG, and we employ a parabolic-pole-face wiggler model for convenience because of its favorable focusing properties. The beam tube radius is assumed to be 0.53 cm. These parameters yield optimal performance for a 1.06 μm wavelength (the high frequency resonance) and a frequency in the neighborhood of 18.74 GHz (the lower frequency resonance for the TE_{11} mode).

The rf accelerating field must be applied, as for tapered wiggler efficiency enhancement, at a point where the bulk of the beam is trapped by the ponderomotive potential but has not undergone a full synchrotron oscillation. Since this depends upon the initial power, we assume that the

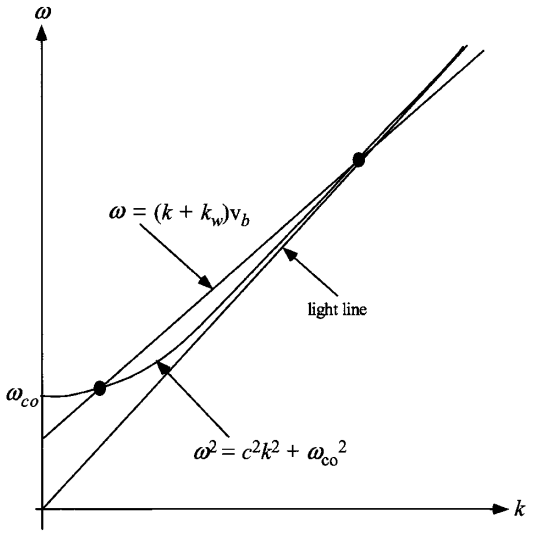

FIG. 1. Schematic illustration of the upper and lower intersections (dots) between the FEL beam resonance line and the dispersion equation in the drift tube.

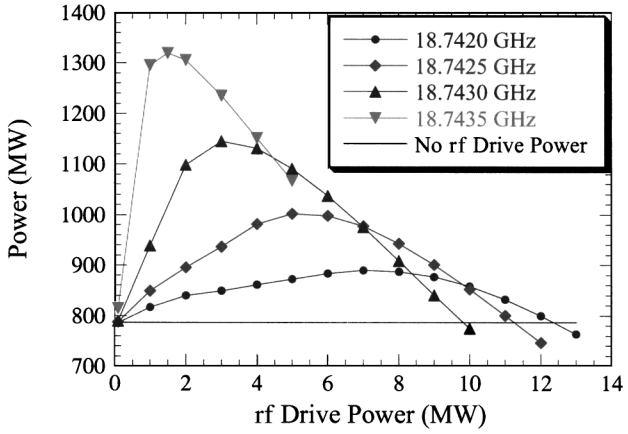

FIG. 2. Output power versus rf drive power for several different drive frequencies.

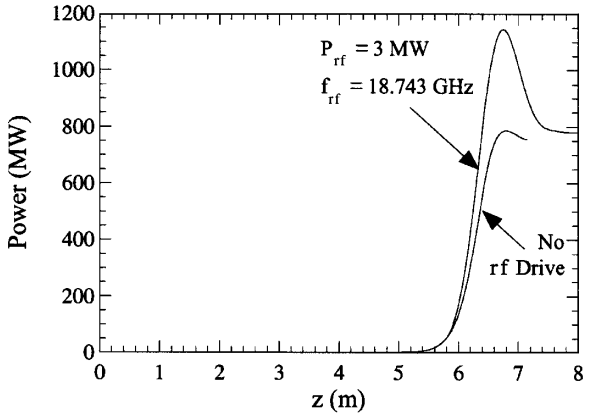

FIG. 3. Power versus distance for the case of no rf drive power for 3 MW of drive power at a frequency of 18.743 GHz.

start power for the 1.06 μm radiation is 100 mW, which yields an optimal point for injection of the rf drive power at about 5.8 m into the wiggler. In an actual amplifier, it may be possible to locate the rf feed in the gap between the jaws of the planar wiggler. Alternately, it may also be convenient to use a two-segment wiggler so that the rf feed can be located in the gap between the wigglers. As far as the simulation is concerned, however, we can inject the power at any point in the wiggler without respect to the details of the injection process.

It is important to note that while we deal with FEL amplifiers here it is also possible to employ them in oscillators. The tapered wiggler efficiency enhancement scheme has limited use in an oscillator because the taper reduces the single-pass gain. Since oscillators employ short wigglers to improve the efficiency (which scales inversely with the number of wiggler periods) having sufficient gain to overcome resonator losses can be difficult when a tapered wiggler is employed. However, the rf acceleration scheme may be able to avoid this problem by the simple expedient of waiting until the oscillator has reached a steady state prior to turning on the rf drive power.

An overview of the results that shows the saturated power versus rf drive power for a range of frequencies is shown in Fig. 2, including a line showing the saturated power in the limit of no rf drive power. The maximum efficiency enhancements occur for the higher frequencies studied, and there is an optimal drive power for any given frequency. At drive powers below this optimal value, there is not enough acceleration to completely compensate for the energy lost by the beam, and at higher drive powers the beam is accelerated at a rate faster than the energy loss due to the interaction.

The evolution of the power versus distance with no rf drive power and for a TE_{11} mode rf drive signal at a frequency of 18.743 GHz and a drive power of 3 MW (the optimal case at this frequency) is shown in Fig. 3, where saturation occurs after 6.75 m at a power level of 1146 MW. This contrasts with a saturated power of 787 MW in the absence of the rf drive. This represents an increase of 46% over the saturated power in the absence of rf drive power, and it occurs over a slightly shorter interaction length.

The spent beam distributions for these cases are shown in Fig. 4. It is clear that the energy spread with no drive power (a) is only marginally different from that when the rf drive power is applied (b). In contrast to the effect of the tapered wiggler, the rf drive mechanism does not result in a significant change in the energy of the spent beam.

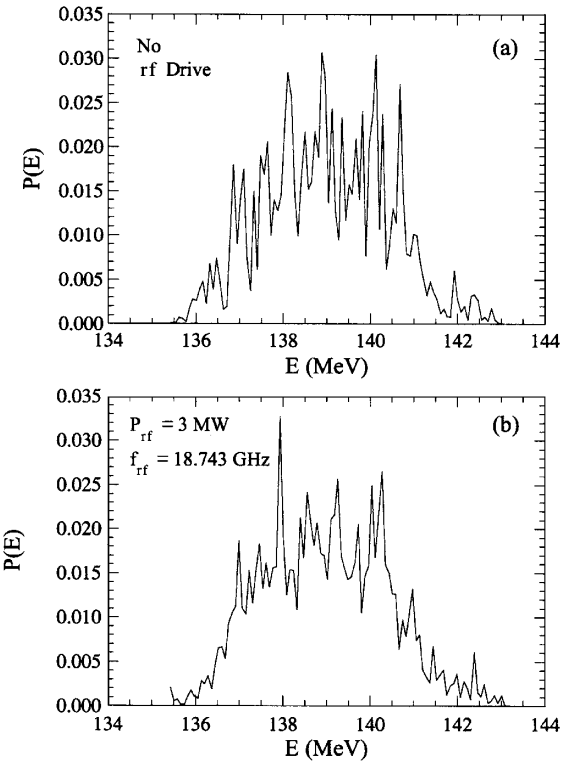

FIG. 4. Spent beam distributions for the case of no rf drive power (a) and for 3 MW of rf drive power at a frequency of 18.743 GHz (b) corresponding to the cases shown in Fig. 2.

The aforementioned example with an rf drive frequency at 18.743 GHz exhibited pump depletion as the radiation at 1.06 μm was amplified. However, an anomalous effect has been observed at the higher frequencies for the rf drive signal. Specifically, at frequencies above 18.743 45 GHz we find that there is no pump depletion. Instead, both the pump wave and the short wavelength resonant wave are amplified, and a double-peaked beam distribution is formed. What is happening is that the low frequency rf drive signal accelerates part of the beam that maintains the high frequency/short wavelength resonance but also decelerates another part of the beam that amplifies the rf drive signal. An example of the spent beam distribution in this regime is shown in Fig. 5, for an rf drive frequency of 18.7435 GHz and the optimal drive power of 1.5 MW (see Fig. 2). Observe that while the distribution has a double peak, the overall energy spread is still not significantly greater than was found in the absence of rf drive power [Fig. 4(a)].

To summarize, we have described a new efficiency enhancement concept using concurrent rf acceleration with the amplification of the short wavelength FEL interaction. The difference with previously proposed rf acceleration schemes is that this mechanism makes use of the low frequency FEL resonance in a smooth-bore drift tube as an inverse-FEL accelerator; hence, it does not require large slow-wave accelerating cavities. Simulations show that substantial enhancements in the efficiency are possible with a relatively small effect on the overall spent beam energy spread. In addition, an anomalous regime has been identified where both the high and low frequency waves are amplified, which results in a double-peaked spent beam distribution but with a relatively benign effect on the overall energy spread. The question of the energy spread is of prime importance because high average power FELs are most likely to be designed with an energy recovery system in order to enhance the overall "wallplug" efficiency, and the effectiveness of such energy recovery systems depends upon a low beam energy spread. The rf drive frequency can be tailored by the proper selection of the transverse dimensions of the drift tube for any given choice of beam and wiggler parameters.

Finally, there are several practical issues involved in the implementation of this concept. First, the implementation of the concept must take into account the available rf source technology in the narrow frequency range of interest, which is dictated primarily by the beam tube size. This is dictated, in turn, by the beam and wiggler parameters and by the wiggler gap size needed to achieve any specified field amplitude. The technique is applicable to any desired wavelength although, at the present time, interest centers on infrared FELs. However, it should be noted that the most important determinant of the rf frequency is the diameter of the drift tube. Second, this Letter dealt with FEL amplifiers, which raises the question of whether the input coupler can be inserted between the jaws of a planar wiggler. To this end, a rectangular drift tube may facilitate the design of input couplers, and we note that the formulation described herein can be readily generalized to rectangular drift tubes. However, a segmented wiggler can also be used and the input coupler inserted in the gap between the wigglers. Third, this concept can also be used in oscillators with the input coupler located upstream from the wiggler entrance. The rf drive power would be turned on only after the oscillator has reached a steady state. In this way the small signal gain will not be negatively impacted. Fourth, wakefields generated as the beam traverses the input coupler can, in principle, degrade beam quality and this issue must be studied. Fifth, rf losses in the drift tube can also affect the overall interaction efficiency and must be included in the modeling effort. Last, the efficiency enhancement found in the present set of simulations does not constitute the ultimate limit on the saturation efficiency.

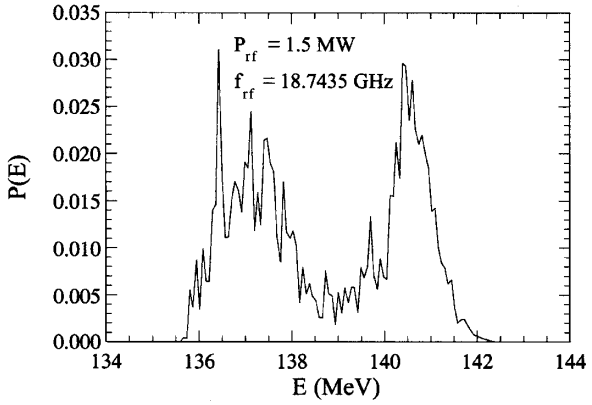

FIG. 5. Spent beam distribution of the anomalous regime where both the high and low frequency waves are amplified.

The authors acknowledge helpful discussions with Dr. Bruce Danly. This work was supported by a Phase I Small Business Innovative Research Contract from the Naval Surface Warfare Center, Dahlgren, VA.

[1] H. P. Freund and T. M. Antonsen, Jr., *Principles of Free-electron Lasers* (Chapman & Hall, London, 1996), 2nd ed.
[2] P. G. O'Shea and H. P. Freund, Science **292**, 1853 (2001).
[3] LCLS Design Group, LCLS Design Report, National Technical Information Service Document No. DE98059292, Springfield, VA, 1998.
[4] J. Rossbach, Nucl. Instrum. Methods Phys. Res., Sect. A **375**, 269 (1996).
[5] G. R. Neil *et al.*, Phys. Rev. Lett. **84**, 662 (2000).
[6] P. Sprangle and C. M. Tang, AIAA J. **19**, 1164 (1981).
[7] A.H. Ho *et al.*, IEEE J. Quantum Electron. **23**, 1545 (1987).
[8] J. F. Schmerge *et al.*, Nucl. Instrum. Methods Phys. Res., Sect. A **341**, 335 (1994).
[9] H. P. Freund *et al.*, IEEE J. Quantum Electron. **36**, 275 (2000).